ADVANCED HEALTHCARE MATERIALS
www.advhealthmat.de

Immunomodulation With Local, Sustained Delivery of Pituitary Adenylate Cyclase Activating Polypeptide Results in Improved Functional Recovery in Stroke-Injured Mice

*Eric Ho, David Xinzheyang Li, Hong Cui, Dania Akbar, Ricky Siu, Cindi M. Morshead, David Chatenet, and Molly S. Shoichet**

Following ischemic stroke, astrocytes and microglia become activated and create a hostile microenvironment that can exacerbate brain damage, yet these cells also contribute to tissue regeneration. Pituitary adenylate cyclase activating polypeptide (PACAP) is a promising neuroprotective peptide that modulates microglia toward a pro-reparative phenotype, however, its short half-life in vivo and dose-limited off-target effects have made systemic delivery untenable. Local delivery presents a promising alternative. To this end, we developed a hydrogel-nanoparticle composite for the minimally invasive, local delivery of PACAP to the brain and tested this strategy in chemically-induced, endothelin-1 stroke-injured mice. We demonstrate that prolonged delivery of PACAP improved the physical strength and mobility of mice for up to 28 days after stroke. The treatment decreased the number of apoptotic neurons in the stroke microenvironment, increased neuron survival at 28 days post-stroke, and attenuated reactive astrogliosis and microglia activation. PACAP stimulation resulted in increased Iba1$^+$Arg1$^+$ pro-reparative microglia and decreased Iba1$^+$CD86$^+$ pro-inflammatory microglia. Furthermore, PACAP stimulation significantly decreased pro-inflammatory GFAP$^+$LCN2$^+$ and GFAP$^+$S100β^+ astrocytes versus controls. This phenotypic shift in microglia and astrocytes may account for the functional improvements post stroke and paves the way for local delivery of new therapeutic strategies targeting the immune response for stroke treatment.

1. Introduction

Progress toward treatments for neurological disorders, like ischemic stroke, is challenging due to the difficulties of achieving therapeutically relevant concentrations in the brain. Stroke is a leading cause of permanent adult disability,[1] and to date, no therapeutic strategies except thrombolysis and thrombectomy have been effective in the clinic. Unfortunately, these therapeutic strategies are only effective for a short window of up to 24 h following stroke onset,[2,3] treating less than 6% of stroke patients and leaving them with only rehabilitation therapy. Following a stroke, resident microglia and astrocytes are activated, releasing pro-inflammatory cytokines like TNFα and cytotoxic compounds like reactive oxygen species, which exacerbate the stroke injury, lead to the establishment of a scar, promote edema formation, and draw more immune cells to the site of the infarct.[4–12] Microglia and astrocyte activation can persist for at least 1 month post-stroke. However, these cells have also been shown to resolve stroke progression, releasing

E. Ho, M. S. Shoichet
Department of Chemical Engineering and Applied Chemistry
University of Toronto
200 College Street, Toronto, ON M5S 3E5, Canada
E-mail: molly.shoichet@utoronto.ca
E. Ho, D. X. Li, H. Cui, R. Siu, C. M. Morshead, M. S. Shoichet
Institute of Biomedical Engineering
University of Toronto
164 College Street, Toronto, ON M5S 3G9, Canada
D. Chatenet
INRS – Centre Armand-Frappier Santé Biotechnologie
531 boul. des Prairies, Laval, QC H7V 1B7, Canada
M. S. Shoichet
Department of Chemistry
University of Toronto
80 St. George Street, Toronto, ON M5S 3H6, Canada
R. Siu, C. M. Morshead
Department of Surgery
University of Toronto
149 College Street, Toronto, ON M5S 3E1, Canada
E. Ho, D. X. Li, H. Cui, D. Akbar, R. Siu, C. M. Morshead, M. S. Shoichet
Terrence Donnelly Centre for Cellular and Biomolecular Research
University of Toronto
160 College Street, Toronto, ON M5S 3E1, Canada

The ORCID identification number(s) for the author(s) of this article can be found under https://doi.org/10.1002/adhm.202500765

DOI: 10.1002/adhm.202500765

neurotrophic compounds, sequestering extracellular glutamate, and endocytosing necrotic debris to pave the way for tissue regeneration.[13–19] New strategies aim to enhance the beneficial effects of microglial activation while downregulating the detrimental ones.[20–22] For example, Lu et al. delivered anti-inflammatory minocycline to stroke-injured mice, which resulted in downregulation of pro-inflammatory genes, upregulation of anti-inflammatory genes, and functional recovery compared to the saline-treated controls.[23] Moreover, Bourget et al. demonstrated that metformin, administered in a model of neonatal stroke in mice, decreased microglia activation and improved behavioral outcomes.[24] We hypothesized that by manipulating the activated resident immune cells after stroke injury, the brain microenvironment would be more conducive for repair.

Pituitary adenylate cyclase activating polypeptide (PACAP), primarily found in its 38 amino acid isoform in the central nervous system (CNS),[25] is a potential therapeutic for stroke treatment with pleiotropic effects in the brain. PACAP gene transcripts are upregulated in the cortex after ischemic injury,[26] and its receptors are localized to neurons, astrocytes, and microglia.[27,28] PACAP is linked to many anti-apoptotic signaling pathways, including PKA/PKC dependent stimulation of Bcl-2 and subsequent inhibition of Cas3/NF-κB, and MAPK/ERK activation through a cAMP dependent pathway.[29] PACAP also directly affects anti-inflammatory properties of microglia[29,30] and indirectly promotes the production of trophic factors in the brain microenvironment, including that of IL-6[31,32] and BDNF,[33] which have been linked to regeneration.

PACAP treatment has been shown to be efficacious in experimental stroke studies, decreasing infarct volume, attenuating inflammation, and improving functional outcomes when delivered either before or a few hours after stroke injury.[29,34–36] However, adaptation of PACAP in the clinic has been limited by both its short half-life and dose-limiting side effects like migraines, vasodilation, and increased end tidal CO_2 pressure.[37,38] In addition, the blood-brain barrier (BBB) prevents a vast majority of compounds in circulation from entering the brain parenchyma. Some groups have explored the local delivery of PACAP to the brain with bolus injections into the ventricles,[39–43] however, these are quickly cleared by cerebrospinal fluid flow, resulting in minimal amounts in the brain parenchyma.[44]

Extended local delivery to the brain obviates the limitations of bolus local and systemic delivery strategies. Interestingly, Brifault et al. showed that embryonic stem cells genetically modified to release PACAP and injected into the brain 3 d after permanent middle cerebral artery occlusion (MCAO) in mice resulted in no difference in lesion volume, but improved functional recovery concomitant with immune modulation.[35] Even though prolonged local release addressed low dosing and off target side effects, embryonic stem cell transplantation is accompanied by several other challenges, including cell survival, immune rejection, and tumorigenesis. Moreover, an invasive strategy, such as that with the embryonic stem cells, may cause further damage to brain tissue and undesirable immune responses to the implanted system. Therefore, due to the quick clearance of bolus PACAP injections, combined with our interest in targeting the immune response for an extended period of time, we designed an innovative strategy for local, minimally-invasive delivery of PACAP to the stroke injured brain to circumvent these limitations and enable, for the first time, the maximum efficacy of PACAP to be tested for stroke treatment.

We describe a biomaterial-based local delivery strategy for PACAP for the treatment of stroke-injured mice. The vehicle utilizes a nanoparticle-hydrogel composite – a physically crosslinked hydrogel composed of hyaluronan (HA) and methylcellulose (MC), and nanoparticles composed of carboxy-terminated poly(lactic-co-glycolic acid) (PLGA). MC gels via hydrophobic interactions at elevated temperatures, and HA lowers the gelation temperature to 37 °C via the salting out effect while also increasing the viscosity of the polymer solution.[45–47] The hydrogel is biocompatible, shear-thinning, and inverse thermal gelling, which enables injection through a fine-gauge needle and thermogelation at the site of injection.[48] Encapsulation of protein therapeutics in PLGA nanoparticles is typically used to control therapeutic protein release; however, we achieved controlled release of this peptide through tuned electrostatic surface interactions[46,49] between negatively charged, blank PLGA nanoparticles and positively charged PACAP. By manipulating these interactions, we achieve electrostatic-adsorption controlled release without encapsulation and the associated drawbacks.[50,51] We explored the viability of this PACAP delivery strategy and evaluated the effects of prolonged, biomaterial-delivered PACAP stimulation on the stroke-injured mouse brain.

The hydrogel-nanoparticle composite was applied epicortically –, i.e., directly onto the cortex at the cortical stroke lesion site after endothelin-1 (Et-1) stroke injury in mice. Et-1 is a vasoconstrictive peptide that, when injected at specific coordinates in the brain, causes local constriction of the surrounding blood vessels. This ischemia is transient and is followed by reperfusion,[52] which closely resembles the events that occur in the human brain.[53] We evaluated efficacy with both behavioral studies and immunohistochemistry (**Figure 1**). We demonstrate functional forelimb recovery of the injured mice 1 month post stroke after prolonged local PACAP delivery. Importantly, we saw a decrease in apoptosis of ischemic neurons in the stroke microenvironment in the first week after stroke insult, and decreased infarct volume and increased neuron survival 1 month post stroke. During the 2 weeks post-injury, we observed a reduction in both astrocyte and microglia activation, and that $CD86^+$ pro-inflammatory microglia decreased while $Arg1^+$ pro-reparative ones increased. Additionally, pro-inflammatory astrogliosis was significantly decreased in PACAP-treated animals up to 2 weeks post-injury, as demonstrated by a decrease in $LCN2^+$ and $S100\beta^+$ astrocytes. We demonstrate that the anti-inflammatory and neuroprotective effects of PACAP on the microenvironment correlate with functional recovery and tissue repair of stroke-injured mice.

2. Results

2.1. HAMC-PLGA Nanocomposite Material Characterization

We describe a biomaterial-based local delivery strategy for PACAP for treatment of stroke-injured mice. The vehicle utilizes a nanoparticle-hydrogel composite – a physically crosslinked hydrogel composed of hyaluronan (HA) and methylcellulose (MC), and nanoparticles composed of carboxy-terminated poly(lactic-co-glycolic acid) (PLGA). HAMC gels in 19 min, whereas the composite gels at 57 min, possibly because the nanoparticles

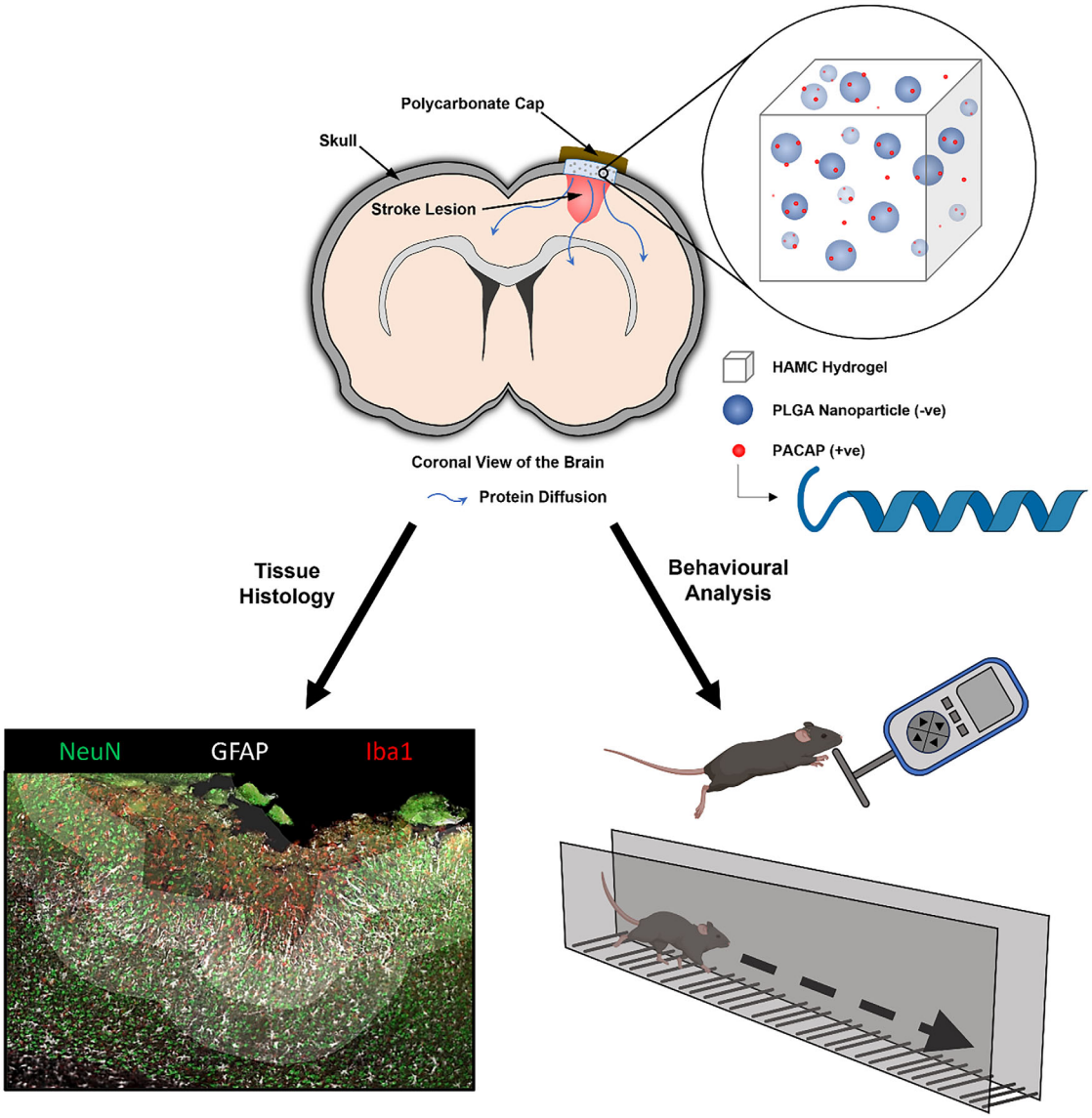

Figure 1. Implantation strategy for the local delivery of PACAP to the stroke-injured brain and analyses. Schematic of epicortical delivery strategy of PACAP to the stroke injured mouse brain. Recovery was assessed by histological analysis of the tissue and behavioral outcomes after treatment.

disrupt the hydrophobic interactions between methylcellulose. Both HAMC and PLGA-loaded HAMC are soft gels, with a storage modulus 226 ± 44 Pa and 163 ± 31 Pa, respectively, which should be compatible with that of brain tissue. The injectability of the material was also characterized by measuring the peak force required to expel the gel from a 26-gauge needle that was used in surgery. Due to their shear thinning properties, both HAMC and PLGA-loaded HAMC were injectable for at least 30 h, with a force between 12–15 N. This is much less than the 30 N limit for injection by hand.[54] In an accelerated degradation study with hyaluronidase, we observed degradation within 7 days (Figure S3, Supporting Information). Previously, this composite has been shown to be biocompatible and to sustain the release profile of PACAP over 2 weeks.[46]

2.2. Epicortical Delivery of PACAP Improves Motor Recovery

Mice were tested with two behavioral tasks (timeline shown in **Figure 2**A): horizontal ladder traverse tested complex motor coordination by assessing forepaw slippage while grip strength measured the overall forelimb strength. Mice were tested the day before stroke injury (t = -1 d) in both tasks to establish baseline behavior. Mice received an Et-1 induced focal ischemic stroke injury on day 0, targeting the forelimb motor cortex to elicit functional motor deficits therein.[55,53] Then 3 µL of the drug loaded hydrogel nanocomposite (with 1 µg of PACAP) was applied to the cortical surface of the brain. The skull was then sealed with a polycarbonate cap, and the skin sutured closed (Schematic in Figure 1). Two days post ischemia (2 dpi), the mice were tested

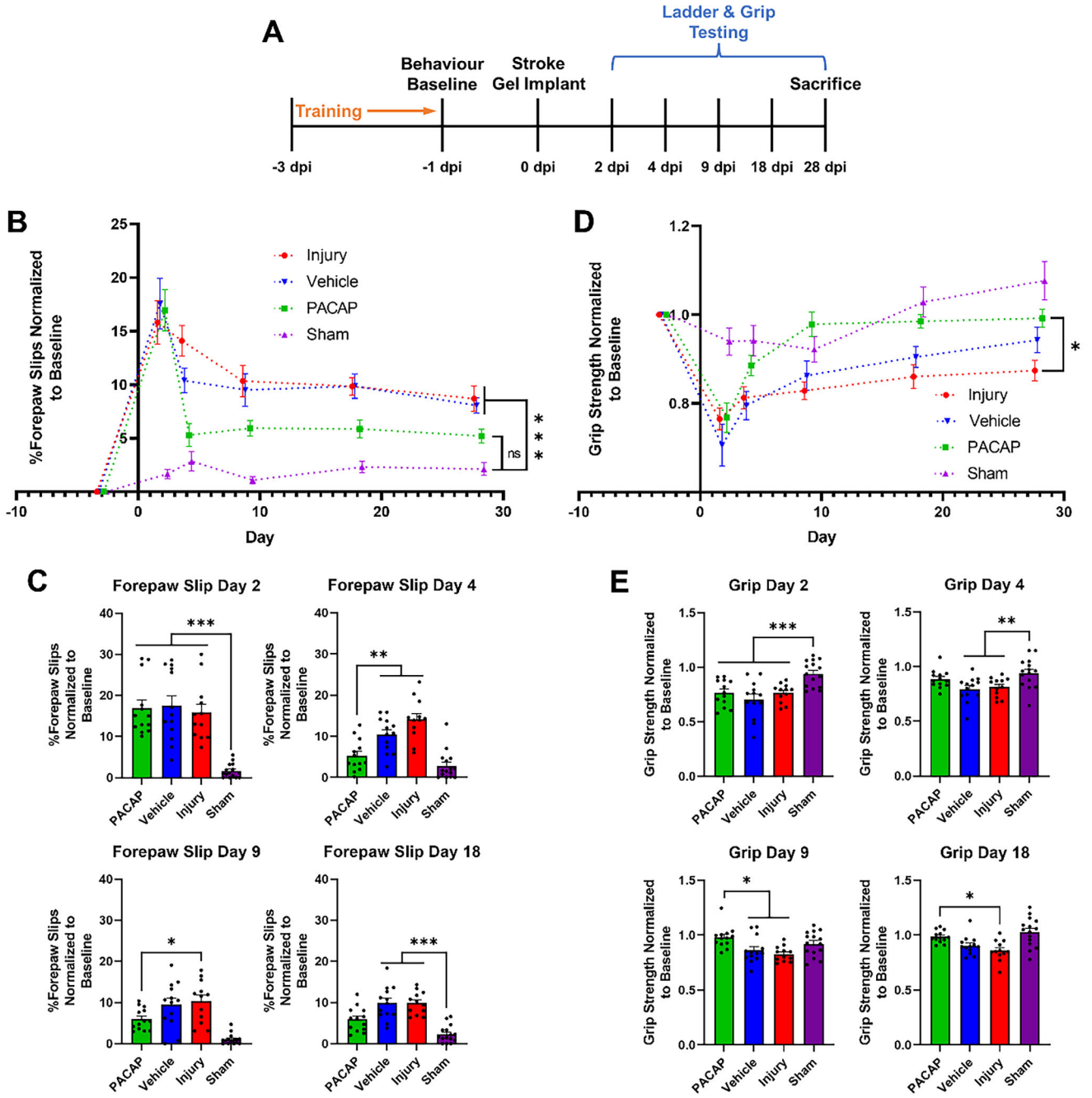

Figure 2. Local PACAP delivery improves the functional recovery of stroke-injured mice. A) Timeline of behavioral testing paradigm B) Quantification of forepaw slips normalized to each mouse's pre-stroke slip rate over 28 d (statistics shown for the final, 28 d timepoint). C) Timepoint comparisons of forepaw slips from (A). PACAP treatment demonstrates significant improvement at 4 and 9 dpi, and similarity to the sham at 18 and 28 dpi. D) Quantification of grip strength normalized to each mouse's pre-stroke grip strength over 28 d (statistics shown for the final, 28 d timepoint). E) Timepoint comparisons of grip strength from (C). PACAP demonstrates significant improvement versus the vehicle group at 9 dpi, and the injury group at 9, 18, and 28 dpi. Data are expressed as mean + SEM, and all data points represent individual mice (n = 12 for Injury, $n = 13$ for PACAP and Vehicle, $n = 15$ for Sham). Significance evaluated by a two-way repeated measures ANOVA with Tukey's post-hoc test, $^{*}P<0.05$, $^{**}P<0.01$, $^{***}P<0.001$.

again and compared to their baseline behavior, mice that did not exhibit a functional deficit during ladder traverse in forepaw slips less than 1 standard deviation of their baseline were excluded. All groups included in the study displayed a significant impairment in motor function compared to sham mice at 2 dpi in both behavioral tests – horizontal ladder traverse forepaw slips and grip strength – validating the Et-1 stroke injury model.

In the horizontal ladder test, PACAP treatment significantly decreased forepaw slippage (Figure 2B,C). PACAP treated mice showed significant recovery compared to both injury and vehicle

groups ($p<0.0001$ and $p = 0.0055$, respectively) at 4 dpi and compared to the injury group ($p = 0.0261$) at 9 dpi. By day 18 (and to our testing endpoint of 28 dpi), PACAP treated mice were not significantly different from sham mice in terms of forepaw slips, indicating functional recovery. In contrast, both the vehicle and injury groups exhibited significantly more slips than the sham.

In the grip strength task (Figure 2D,E), PACAP treated mice were not significantly different from the sham at 4 dpi, whereas the injury and vehicle groups exhibited a significant deficit ($p = 0.0061$ and $p = 0.0009$, respectively), suggesting functional recovery. At later timepoints PACAP treated mice displayed accelerated recovery in the grip strength test with significant effects at 9 dpi versus the vehicle alone ($p = 0.0198$) and at 18 and 28 dpi versus the injury group ($p = 0.0120$ and $p = 0.0204$, respectively). Based on both tasks, local PACAP delivery to the stroke-injured brain improved motor recovery as early as 4 dpi and persisted at least until 28 dpi.

2.3. Controlled release of PACAP Decreases Apoptosis and Infarct Volume

Functional recovery after stroke depends on many different factors, such as supporting neural cell survival, encouraging neurogenesis, modulating the inflammatory response, and promoting neural plasticity, among others. To examine the cellular response to PACAP treatment and its correlation with functional recovery, we assessed neuroprotective effects by both counting $TUNEL^+$ cells to quantify the extent of apoptosis in the stroke microenvironment and measuring infarct volume, with the infarct boundary defined as the transition from dense NeuN staining to sparse/no NeuN staining (i.e., the $NeuN^{dense}$ to $NeuN^{sparse}$ border). We characterized $TUNEL^+$ and $TUNEL^+NeuN^+$ cells for the first week post injury, as apoptosis mainly occurs in the acute phase. We characterized infarct volume at 4 dpi for the acute phase and then 2 and 4 weeks post-injury, when the infarct has stabilized. At 4 dpi, PACAP treated mice had fewer $TUNEL^+$ cells compared to both injury ($p = 0.0317$) and vehicle ($p = 0.0586$) groups (**Figure** 3A,B) and fewer $TUNEL^+NeuN^+$ cells at 4 dpi compared to both injury ($p = 0.0417$) and vehicle ($p = 0.0334$) groups (Figure S4, Supporting Information). This correlated with neuron counts at 4 dpi, which were not significantly different between groups (Figure S5, Supporting Information). Infarct volume at 4 dpi was somewhat decreased in PACAP treated mice compared to other groups, however this effect was not significant (Figure S6, Supporting Information). By 7 dpi, the $TUNEL^+$ and $TUNEL^+NeuN^+$ cell count was still lower in PACAP treated mice, although not significantly compared to other groups (Figures S4 and S7, Supporting Information for $TUNEL^+NeuN^+$ and $TUNEL^+$ staining, respectively). PACAP treatment also significantly decreased infarct volume compared to the injury group at 14 and 28 dpi ($p = 0.0054$ and $p = 0.0127$, respectively), displaying its neuroprotective effects through the preservation of neurons at these later timepoints (Figure 3C,D). Similarly, PACAP treatment significantly increased neuron counts compared to the injury group at 14 and 28 dpi ($p = 0.0427$ and $p = 0.0002$, respectively) (Figure S5, Supporting Information). The decreased infarct volume and increased neuron survival may have contributed to the functional improvements observed in PACAP-treated mice.

2.4. Biomaterial-Delivered PACAP Attenuates Glial Cell Activation

We wondered whether local deliver of PACAP would alter the activation of microglia and astrocytes, in addition to its known neuroprotective effects on neurons, after stroke injury. Coronal brain sections were stained with NeuN, Iba1, and GFAP. The $NeuN^{dense}$ to $NeuN^{sparse}$ border was used to identify the boundary of the infarct region of interest (ROI), as previously described, which was then expanded in two 250 µm increments, creating two perilesional ROIs: 0–250 µm from the infarct and 250–500 µm from the infarct, thereby resulting in three spatially-defined stroke microenvironments: infarct, 0–250, and 250–500 ROIs. We stained for $Iba1^+$ microglia and $GFAP^+$ astrocytes (**Figure** 4A, individual channels in Figure S8, Supporting Information). At 4 dpi, we observed that PACAP treatment significantly decreased Iba1 expression compared to the injury group in all 3 ROIs (Figure 4B,C) (full size images in Figure S9, Supporting Information). At 7 dpi, the effect of PACAP on Iba1 expression was less pronounced than those at 4 dpi and significant at $p<0.1$, but not significant at $p<0.05$, we observed reduced Iba1 expression compared to the injury group in the infarct ROI ($p = 0.0513$) and in the 0–250 ROI ($p = 0.0781$) (representative images Figure S10, Supporting Information). At 10 and 14 dpi no significant differences between groups were observed, with Iba1 expression decreasing over time (Figure S11, Supporting Information). At 28 dpi, while there was still some microglia activation in the infarct, there were no significant differences between groups at 28 dpi (Figure 4C, representative images Figure S12, Supporting Information).

At 4 dpi, PACAP treatment significantly decreased GFAP expression compared to the injury ($p = 0.0012$) and vehicle ($p = 0.0054$) groups in the infarct and compared to the injury in the 0–250 and 250–500 ROIs ($p<0.001$ for both, Figure 4B,D). Interestingly, the difference in GFAP+ astrocyte expression between injury and vehicle treated mice was lower but not significant at $p<0.05$ in the 0–250 ROI ($p = 0.0692$) and not different in the 250–500 ROI. Combined with trends observed with Iba1 expression, where the vehicle moderately decreased Iba1 staining, this suggests that the vehicle had an added anti-inflammatory impact on the tissue response, which is consistent with previous studies using the HAMC hydrogel delivery vehicle.[56] At 7 dpi, PACAP decreased GFAP expression in all ROIs compared to the injury and vehicle groups, however, the only significant effect was observed in the 0–250 ROI between PACAP and injury ($p = 0.0138$, representative images Figure S10, Supporting Information). Similar to Iba1, GFAP expression decreased over time to 28 dpi (Figure S11, Supporting Information), with no significant differences observed between 10 and 28 dpi (representative images Figure S12, Supporting Information). Overall, both microglia and astrocyte activation decreased with our slow release PACAP treatment in the early timepoints after stroke injury, with the initial attenuated response, possibly contributing to the reduced infarct volume and improved functional recovery.

2.5. PACAP Treatment Increases Arg1 Expression and Decreases CD86 Expression in $Iba1^+$ Microglia

To further characterize the microglial response to PACAP treatment, we stained for CD86, which is expressed in

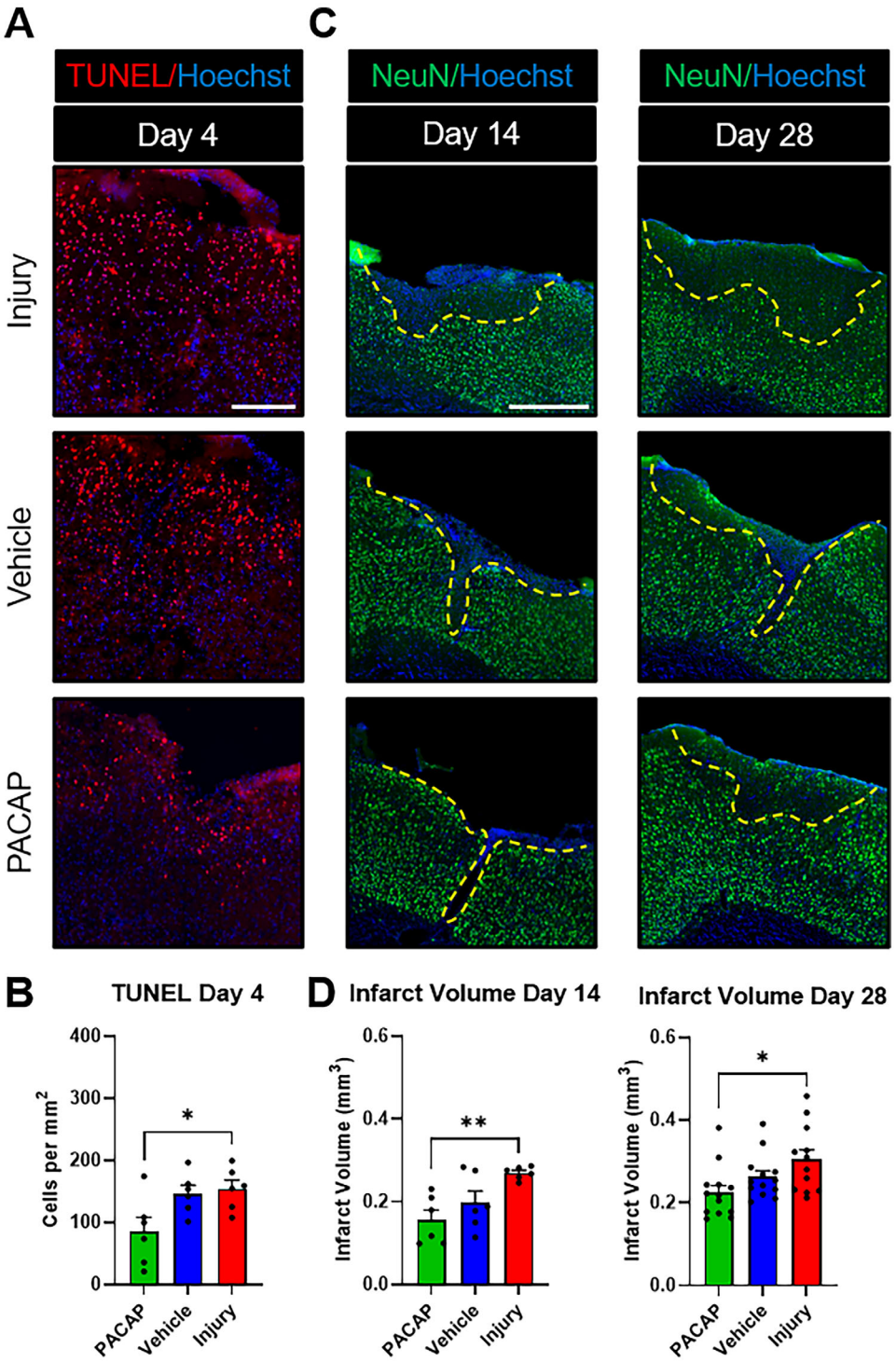

Figure 3. PACAP treatment decreases cell apoptosis and infarct volume in the stroke-injured mouse brain. A) Representative images of TUNEL^{+} apoptotic cells in the stroke-injured brain. Scale bar is 200 µm. B) Quantification of TUNEL^{+} cells at 4 dpi, demonstrating a significant decrease in apoptotic cells with PACAP treatment. C) Representative images of stroke-injured mouse brains with the infarct boundary defined at the border of NeuN^{dense} to NeuN^{sparse}, outlined in yellow at 14 and 28 dpi. Scale bar is 500 µm. D) Quantification of stroke infarct volume at 14 and 28 dpi, demonstrating decreased infarct volume in PACAP treated mice. Data are expressed as mean + SEM, and all data points represent individual mice (4 dpi: $n = 6$ for all groups, 14 dpi: $n = 6$ for all groups, 28 dpi: $n = 12$ for Injury, $n = 13$ for PACAP and Vehicle). Significance evaluated by a one-way ANOVA with Tukey's post-hoc test, $^{*}P<0.05$, $^{**}P<0.01$.

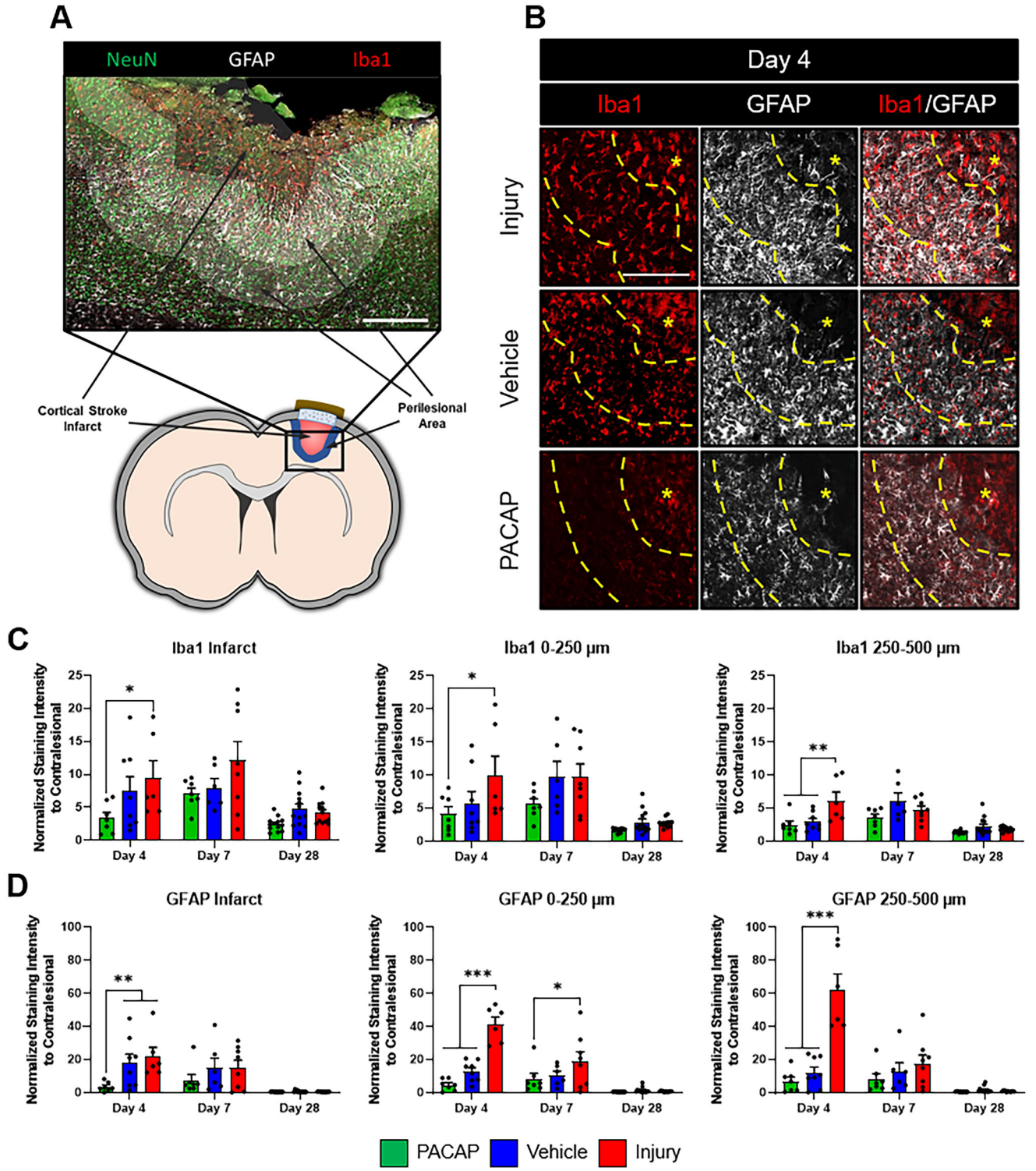

Figure 4. PACAP treatment decreases microglia and astrocyte activation after ischemic stroke. A) Schematic and representative image of infarct and expanded perilesional areas. Scale bar is 500 µm. B) Representative images of Iba1 and GFAP staining at 4 dpi. Infarct ROI identified with (*) and the infarct ROI border and 0–250 µm ROI border identified with the yellow outlines. Scale bar is 200 µm. C) Quantification of Iba1 staining in the infarct, 0–250 µm, and 250–500 µm perilesional areas, demonstrating PACAP stimulation decreased Iba1 expression in all ROIs at 4 dpi. D) Quantification of GFAP staining in the infarct, 0–250 µm, and 250–500 µm perilesional area, demonstrating PACAP stimulation decreased GFAP expression in all ROIs at 4 dpi and in the 0–250 µm perilesional area at 7 dpi. Data are expressed as mean + SEM and all data points represent individual mice (4 dpi: $n = 7$ for PACAP, $n = 8$ for Vehicle, $n = 6$ for Injury, 7 dpi: $n = 7$ for PACAP, $n = 6$ for Vehicle, $n = 8$ for Injury, 28 dpi: $n = 12$ for Injury, $n = 13$ for PACAP and Vehicle). Significance evaluated by a two-way ANOVA with Tukey's post-hoc test, $^{*}P<0.05$, $^{**}P<0.01$, $^{***}P<0.001$.

pro-inflammatory microglia, and Arg1, which is expressed in pro-reparative microglia. Colocalized staining with Iba1 was used to identify microglia, and the ROI was based on Iba1$^+$ ameboid microglia. Arg1$^+$Iba1$^+$ microglia staining was not different between groups at 4 dpi (representative images in Figure S13, Supporting Information). PACAP treatment significantly increased pro-reparative Arg1$^+$Iba1$^+$ microglia compared to both the injury ($p = 0.0008$) and vehicle ($p = 0.006$) groups at 7 dpi (**Figure 5**A–C, full size images in Figure S14, Supporting Information), which remained significant at 10 dpi relative to injury ($p = 0.0331$, representative images in Figure S15, Supporting Information), however, at 14 and 28 dpi, there were no significant differences between groups (Figure S16, Supporting Information). Importantly, pro-inflammatory CD86$^+$Iba1$^+$ microglia decreased in PACAP treated mice compared to the injury group at 4 dpi ($p = 0.0526$, representative images in Figure S13, Supporting Information) and 7 dpi ($p = 0.0874$, full size images in Figure S14, Supporting Information), with a significant decrease observed at 10 dpi ($p = 0.0473$, representative images in Figure S15, Supporting Information). At 14 dpi CD86$^+$Iba1$^+$ microglia expression was markedly decreased in all groups, while there were no significant differences between groups, PACAP was still the lowest. By day 28 there were no differences in CD86$^+$Iba1$^+$ microglia expression between groups (Figure S16, Supporting Information). These data indicate that PACAP-treated, stroke-injured mice have more pro-reparative and fewer pro-inflammatory microglia than controls within the first 7–10 dpi, which may have contributed to the functional benefits observed.

2.6. PACAP Treatment Decreased LCN2 and S100β Expression in GFAP$^+$ Astrocytes

To further characterize the astrocyte response, we stained for LCN2 and S100β, two markers expressed by reactive astrocytes under pro-inflammatory conditions. Colocalization analysis was used to determine the co-expression of these markers with GFAP$^+$ astrocytes in the stroke microenvironment. PACAP treatment resulted in minimal expression of GFAP$^+$LCN2$^+$ across the study duration with significantly lower expression compared to the injury group at 4 dpi ($p = 0.0013$) and both injury ($p = 0.0053$) and vehicle ($p = 0.0369$) groups at 10 dpi (**Figure 6**A–C). Although no significant differences were observed at the other time points, trends suggest that the LCN2 was expressed the least in PACAP-treated animals, followed by vehicle, then injury. GFAP$^+$S100β^+ staining showed a robust and significant decrease in expression for PACAP treatment compared to both vehicle and injury groups at every time point up to 14 dpi ($p<0.01$ for comparisons between vehicle or injury at the same timepoint, Figure 6A,B,D). PACAP treatment significantly reduced the expression of pro-inflammatory markers from GFAP$^+$ astrocytes as early as 4 dpi, with effects lasting up to 14 dpi. Interestingly, co-labelled GFAP$^+$LCN2$^+$ and GFAP$^+$S100β^+ astrocytes both appear to peak at 10 dpi, which may be attributed to the increased astrogliosis that contributes to the formation of the astrocytic border. However, by 28 dpi, there was reduced expression for both markers, and no differences were observed between the treatment groups, suggesting an expected stabilization of the glial response (Figure S17, Supporting Information). Overall, these data indicate that PACAP-treated, stroke-injured mice have fewer pro-inflammatory astrocytes than controls, which may have led to the observed functional improvements.

3. Discussion

Designing an effective stroke therapy remains challenging due to the instability of many protein therapeutics and the biological barriers inhibiting access to the brain parenchyma with systemically delivered drugs.[57,58] Here, we demonstrated that the local, controlled release of PACAP from a biomaterial nanocomposite resulted in a marked increase in functional recovery in treated mice up to the terminal 28 dpi timepoint compared to injury only mice, and 9 dpi compared to vehicle-only mice. We ascribe the added benefit of the vehicle to the high molecular weight HA used in the hydrogel-nanoparticle composite, which has been shown to have some neuroprotective effects on the stroke microenvironment itself,[59,60] and may explain the moderate improvements of the vehicle-treated mice compared to the injury-only groups. HA has been shown to be anti-inflammatory by antagonizing receptors on immune cells, attenuating immune cell activation, infiltration, and migration.[61,62] This may indicate a possible additive effect of high molecular weight hyaluronan and PACAP on the inflammatory response after stroke injury. The material is also well suited for CNS applications: it is biocompatible, shear thinning for easy injection, fast gelling in situ, and bioresorbable.[47,48,63] The anti-inflammatory action of HA and the ability to manipulate adsorption kinetics between PACAP and the PLGA nanoparticles allow us to target the time-sensitive inflammatory cascade.[45,46,64] Notably, the combination of the hydrogel-nanoparticle composite allows us to achieve the desired mechanical properties of the bulk suspension via the HA and MC chains, while orthogonally controlling release rate by tuning adsorption kinetics to the PLGA nanoparticles. This system offers advantages over hydrogel-only vehicles which cannot normally disentangle release kinetics from mechanical properties. Furthermore, unlike the pro-inflammatory gelatin-norbornene nanofibrous hydrogel used to deliver growth factors when injected into the brain,[65] our anti-inflammatory HAMC nanoparticle composite controls the release of PACAP and is injected on top of the brain cortex. This immunomodulatory strategy is less invasive while benefiting from the simplicity of physically crosslinked gel. Importantly, improvements in both motor control, which is necessary for daily movement, and overall limb strength were observed, which we attribute to the local delivery of PACAP with the hydrogel-nanoparticle composite. These effects were correlated with a decrease in neuronal apoptosis in the acute phase after stroke, as shown by a significant decrease in TUNEL$^+$ and TUNEL$^+$NeuN$^+$ cells. Due to the lag in the PACAP release profile that does not peak until 4 dpi in vivo,[46] infarct volume at 4 dpi only demonstrated a decreasing trend in PACAP treated animals. Apoptosis before this timeframe may not have been significantly affected. The reorganization and stabilization of the infarct in the sub-acute repair phase due to the extended release of PACAP was demonstrated by a significant decrease in infarct volume and a significant increase in neuron cell counts at 14 and 28 dpi in animals that received PACAP. We show, for the first time, that with prolonged PACAP release from a biomaterial delivery vehicle, neuroprotection, extended immune modulation, and

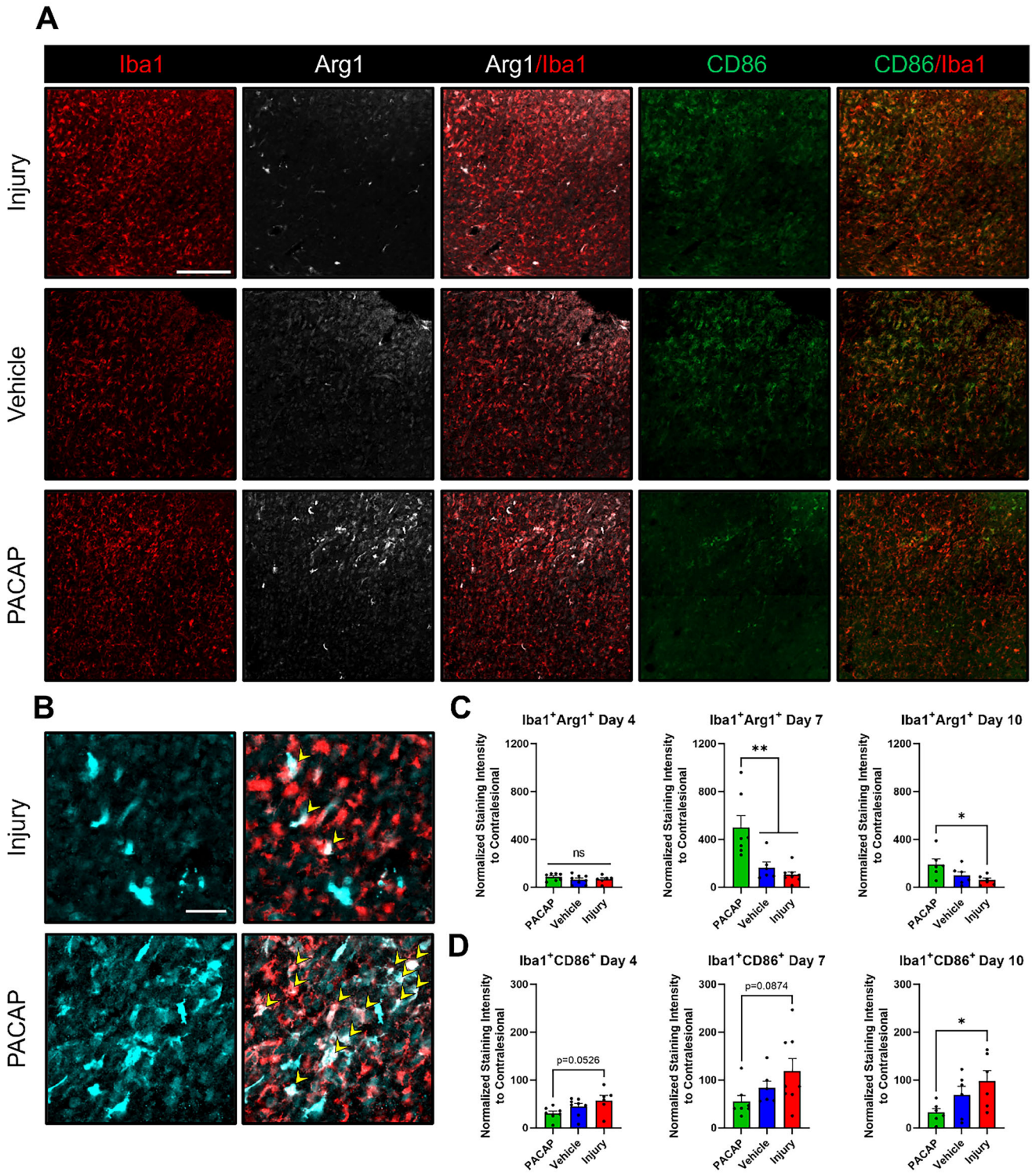

Figure 5. PACAP treatment modulates microglia cell activation. A) Representative images of Iba1, Arg1, and CD86 staining at 7 dpi. Scale bar is 200 µm. B) High magnification images of colocalized Iba1$^+$Arg1$^+$ microglia, identified with yellow arrows. Arg1 staining is false coloured to teal to better visualize colocalization with Iba1, which are shown as white cells. Scale bar is 50 µm. C) Quantification of Iba1$^+$Arg1$^+$ pro-reparative microglia significantly increased with PACAP treatment versus the vehicle and injury at 7 dpi and versus the injury at 10 dpi. D) Quantification of Iba1$^+$CD86$^+$ pro-inflammatory microglia decreased with PACAP treatment at 4 and 7 dpi, and significantly decreased at 10 dpi versus injury. Data are expressed as mean + SEM and all data points represent individual mice (4 dpi: $n = 7$ for PACAP, $n = 8$ for Vehicle, $n = 6$ for Injury, 7 dpi: $n = 7$ for PACAP, $n = 6$ for Vehicle, $n = 8$ for Injury, 10 dpi: $n = 6$ for all groups). Significance evaluated by a one-way ANOVA with Tukey's post-hoc test, $^*P<0.05$, $^{**}P<0.01$.

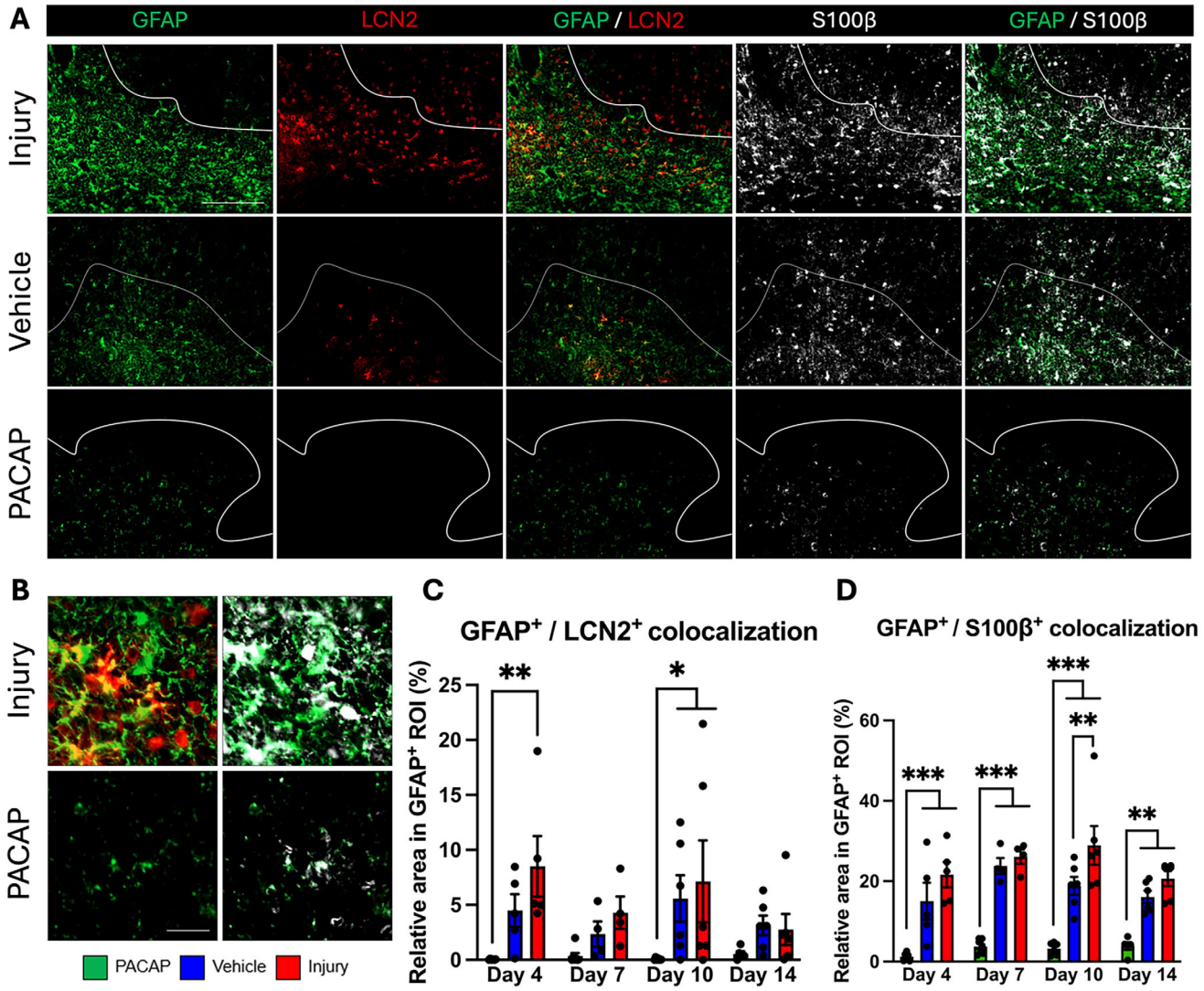

Figure 6. PACAP treatment attenuates pro-inflammatory astrocyte activation. A) Representative images of GFAP, LCN2, and S100β staining at 4 dpi. Scale bar is 200 µm. B) High magnification images of colocalized GFAP$^+$LCN2$^+$ and GFAP$^+$S100β^+ astrocytes. Scale bar is 20 µm. C) PACAP treatment significantly reduced GFAP$^+$LCN2$^+$ astrocytes versus injury at 4 dpi and versus vehicle and injury at 10 dpi. D) PACAP treatment significantly decreased GFAP$^+$S100β^+ astrocytes versus vehicle and injury from 4 to 14 dpi. Data are expressed as mean + SEM and all data points represent individual mice (4 dpi: $n = 6$ for PACAP, $n = 5$ for Vehicle, $n = 5$ for Injury, 7 dpi: $n = 7$ for PACAP, $n = 4$ for Vehicle, $n = 4$ for Injury, 10 dpi: $n = 6$ for all groups, 14 dpi: $n = 5$ for PACAP, $n = 6$ for Vehicle, $n = 6$ for Injury). Significance evaluated by two-way ANOVA with Tukey's post-hoc test, $^*P<0.05$, $^{**}P<0.01$, $^{***}P<0.001$.

therapeutic efficacy were achieved, thereby laying the framework for larger animal studies and ultimately clinical translation.

We probed the tissue response to PACAP delivery to understand how cellular responses correlated with improved functional recovery and neuronal survival. PACAP has a significant anti-inflammatory impact on astrocytes and microglia both in vitro[30,66,67] and in vivo.[32,35,37] PACAP treatment significantly decreased GFAP expression at 4 dpi in all ROIs versus the injury, and in the infarct ROI versus the vehicle. Cherait et al. also showed that intranasal PACAP administration decreased GFAP expression in an MCAO model in mice,[68] which is consistent with our results. While the mechanism has not been investigated, it may be due to downstream activation of PACAP receptors PAC_1, $VPAC_1$, or $VPAC_2$ in astrocytes,[69] or the less cytotoxic and inflammatory stroke microenvironment following PACAP treatment and attenuating their activation. PACAP can improve the survival of astrocytes when challenged with cytotoxic factors, as shown in vitro with reactive oxygen species,[70] which are abundant in the stroke microenvironment.

PACAP treated mice displayed significantly decreased Iba1 expression in the infarct and perilesional areas at 4 dpi, with more modest effects at 7 dpi, indicating that PACAP also reduced microglia activation. PACAP treatment is effective up to 500 µm away from the infarct based on the ROIs assessed, suggesting that the peptide diffuses through the brain to stimulate distal cells. Interestingly, at 4 dpi, Iba1 expression was lower in the vehicle group in the perilesional ROIs, most likely due to the anti-inflammatory effects of HA. Based on Iba1 and GFAP

staining, glial cell activation peaks ≈7–10 dpi in this stroke model, with PACAP and vehicle-treated mice also exhibiting a similar peak. However, unlike injury-only mice, at 4 dpi, PACAP treatment, and to a lesser extent the vehicle, attenuated glial cell activation and proliferation. The decreased neuronal apoptosis during this time, which peaked ≈4 dpi based on $NeuN^+TUNEL^+$ staining, indicated that the stroke microenvironment is less hostile and more regenerative. This timeframe is consistent with the 10-day release of PACAP from the hydrogel-nanoparticle composite, which reaches maximum PACAP concentration in the tissue at 4 dpi.[46] Our data are consistent with reports that show that PACAP protects neural cells and upregulates trophic factors.[33,71,72] The acute phase reduction in glial cell activation observed with our slow-release PACAP treatment may be correlated with the enhanced functional recovery and reduced infarct volume.

While activation of microglia is largely thought to be detrimental to stroke progression, microglia have multiple roles that differentially affect the stroke microenvironment.[9,18,20–22,73] For example, pro-inflammatory microglia generate excessive amounts of cytotoxic species and increase oxidative stress in the stroke microenvironment.[74–76] In contrast, pro-reparative microglia produce anti-inflammatory cytokines,[67,77,78] and neurotrophic factors like GDNF and BDNF,[79] which drive neurogenesis and synaptic plasticity.[80–82] The effect of slow-release PACAP on the microglial response is likely associated with downregulation of pro-inflammatory factors like TNFα, reactive oxygen species, and IL1β,[30,83–85] and upregulation of anti-inflammatory, pro-regenerative factors like IL10 and TGFβ.[35,86] Since PACAP has been shown to modulate the behavior of microglia, we explored two markers, CD86 and Arg1, to better understand microglial behavior. Arg1 expression remained low in the vehicle and injury groups while it increased at 7 and 10 dpi in the PACAP-treated mice. Concurrently, CD86 expression peaked at 10 dpi, which was significantly decreased by PACAP treatment. Interestingly, Iba1 expression is similar between treatment groups at 7 dpi, however, when assessing microglia phenotype, we observed that they expressed more Arg1 and less CD86, suggesting that activated microglia had shifted to a pro-reparative phenotype. Due to the increased functional recovery and tissue regeneration observed in PACAP-treated animals, the increase in Arg1 and decrease in CD86 expression in activated microglia at 7–10 dpi likely had a positive effect on stroke recovery.

Astrocytes play a critical role in the brain, acting as metabolic bridges between neurons and the cerebral vasculature. Astrocytes secrete a variety of different factors such as VEGF, BDNF, and erythropoietin. After stroke, astrocyte activation is generally associated with detrimental impacts on tissue regeneration: astrogliosis contributes to edema formation, secretion of pro-inflammatory cytokines and cytotoxic factors, and the disruption of the BBB from released MMPs and degradation enzymes.[87,88] To further characterize the astrocyte phenotype, we looked at two pro-inflammatory markers, LCN2 and S100β. LCN2 is a glycoprotein secreted by reactive astrocytes under inflammatory conditions and is associated with exacerbated neuronal damage and increased cell apoptosis through the NF-κB pathway, among others.[89,90] S100β can act as an extracellular regulator molecule that at low, physiological concentrations, protects neurons against apoptosis and negatively regulates glial cells against neurotoxic agents.[91] However, at increased expression levels, it can cause cell death and exhibits damage-associated molecular pattern (DAMP)-like properties. Elevated S100β expression in astrocytes has been associated with neuronal damage as well as various neurodegenerative disorders such as Alzheimer's disease, Parkinson's disease, and multiple sclerosis.[92] In our study, PACAP treatment decreased $GFAP^+LCN2^+$ staining compared to the injury group at 4 dpi and both injury and vehicle groups at 10 dpi. Furthermore, we saw a robust and significant reduction in $GFAP^+$ S100β^+ in PACAP-treated animals at every time point up to 14 dpi. PACAP treatment significantly reduced the expression of pro-inflammatory markers from $GFAP^+$ astrocytes as early as 4 dpi with effects lasting up to 14 dpi, suggesting that our sustained delivery strategy may play an important role in attenuating the pro-inflammatory phenotype of astrogliosis post-stroke.

The local PACAP delivery system may be effective in neurological disorders beyond stroke, such as multiple sclerosis (experimental autoimmune encephalomyelitis) and Parkinson's disease[93–95] where microglial and astrocyte dysfunction could impact disease progression.[96–98] Additionally, due to the shear-thinning properties of the hydrogel-nanoparticle composite, this material could be injected into deeper lesions of the brain.[48] It has also been shown that PACAP may control some plasticity-mediated rewiring in the chronic phase of stroke injury through the upregulation of BDNF.[33] With our local delivery strategy, other anti-inflammatory and immune modulating strategies could also be used to ellicit functional repair and tissue regeneration in stroke, and neurological disorders more generally.

4. Conclusion

We demonstrate that prolonged, local delivery of PACAP from a hydrogel-nanoparticle composite reduced inflammation and enhanced functional recovery in a mouse model of stroke. PACAP treatment improved forelimb function and strength in stroke-injured mice at 28 dpi. With PACAP treatment, the number of apoptotic cells decreased, as did astrocyte and microglia activation in the acute phase. Microglial responses were modulated to a more pro-reparative phenotype, as demonstrated with increased $Arg1^+Iba1^+$ and decreased $CD86^+Iba1^+$ staining. Further, there was an attenuation of pro-inflammatory astrocyte activation, as shown with decreased $GFAP^+LCN2^+$ and $GFAP^+S100\beta^+$ staining. PACAP treated mice also had a reduced infarct volume relative to controls. These data substantiate the role of PACAP in neuronal survival directly through neuroprotection and indirectly through anti-inflammatory effects. This study provides insights on the timeframe of intervention for immune modulation therapy for stroke treatment, where prolonged PACAP stimulation for 10 days can drive microglia in the stroke microenvironment to promote repair. We expect that this system would be broadly applicable to other neurological disorders affected by microglial dysfunction.

5. Experimental Section

Formulation of PLGA Nanoparticles: Aseptic PLGA nanoparticles were formulated with a water/oil/water double emulsion as previously

described.[46] PLGA was sourced from LACTEL Absorbable Polymers (B6013-1, inherent viscosity 0.15 to 0.25 dl/g in hexafluoroisopropanol, 50:50 lactic:glycolic ratio, carboxylic acid-terminated). Briefly, 120 mg of PLGA and 0.05 wt% Pluronic F-127 NF (BASF) were dissolved in 900 µL of dichloromethane (DCM, Caledon Laboratories) to form the oil phase. 12 mg of bovine serum albumin (BSA, Sigma–Aldrich, A7030) and 3 mg poly-d-lysine (PDL, Sigma-Aldrich, P7886) was dissolved in 100 µL of artificial cerebrospinal fluid (aCSF) [149 mM NaCl, 3 mM KCl, 0.8 mM $MgCl_2$, 1.4 mM $CaCl_2$, 1.5 mM Na_2HPO_4, and 0.2 mM NaH_2PO_4 in deionized (DI) water, pH 7.4] to form the inner aqueous phase. 2.5 wt.% poly(vinyl alcohol) (PVA, Sigma–Aldrich, P8136) was dissolved in DI water to form the outer aqueous phase. The inner aqueous phase and oil phase were then mixed by brief vortexing, followed by probe sonication on ice at 20% amplitude for 10 min (Sonics & Materials, VCX 130). Following this, 3 mL of the outer aqueous phase was added to this primary emulsion, and sonicated again on ice at 30% amplitude for 10 min. The resulting emulsion was then added to a 50 mL hardening bath of 2.5 wt.% PVA in DI water and stirred gently overnight to allow the DCM to evaporate. The next day, the nanoparticles were collected and washed 4 times by probe sonication in DI water followed by ultracentrifugation at 41000 x G, removal of the supernatant, lyophilization, and storage at −20 °C until use.

Formulation of Drug Loaded Hydrogel-Nanoparticle Composite: To prepare the drug loaded delivery vehicle, PLGA nanoparticles at 25 mg mL^{-1} were dispersed in 0.3 mg mL^{-1} PDL in aCSF and bath sonicated for 5 min to ensure a homogenous distribution. Following this, hyaluronan (HA, NovaMatrix, 1.4-1.8×10^6 g mol^{-1}) and methylcellulose (MC, Shin-Etsu, 300 kg mol^{-1}) were added to the solution of nanoparticles such that the final concentration (after addition of protein aliquot) was 1.4 wt.% HA and 3 wt.% MC. This hydrogel-nanoparticle composite was placed horizontally and blended for 4 min in a dual asymmetric centrifugal mixer (FlackTek, DAC 150 FVZ) at max speed (speedmixed), followed by 5 min of centrifugation at 16000 x G for 5 min. This was repeated a minimum of 4 times until the polymer solution was homogenous. The composite was then stored overnight at 4 °C to let bubbles disperse. The next day, an aliquot of PACAP (Echelon Biosciences, 350–35) was added to achieve a final concentration of 0.33 µg $µL^{-1}$ of peptide in the composite. 100 µL of the drug-loaded composite was loaded in a 2 mL microcentrifuge tube and was speedmixed for 10 s vertically, followed by 10 s horizontally, followed by 10 s of centrifugation, and finally speedmixed for 10 s vertically to mix the peptide in the vehicle. For the vehicle-only mice, the composite was formed as described, except without PACAP.

Rheological Properties and Gelation Time: Gelation time was determined using rheology with a rheometer (TA Discovery HR-2) equipped with a 40 mm steel parallel Peltier plate for temperature control. To minimize evaporation during measurements, a solvent trap was utilized. Rheological measurements were conducted at an angular speed of 1 rad/s with 1% strain over 2 h at 40 °C. Briefly, 100 µL of pre-gel HAMC solution with and without PLGA nanoparticles was added to the rheometer and allowed to equilibrate for 30 s at ambient temperature before data acquisition. The rheological data were plotted for shear loss modulus (G″) and shear storage modulus (G′) against time, and the gelation time was determined at the cross modulus, where the storage modulus equates to the loss modulus.

Injectability Test: A 500 µL pre-gel HAMC solution with and without PLGA nanoparticles was prepared and loaded into a 1 mL disposable syringe (BD, slip tip). After equilibrating at ambient temperatures, a 26-gauge needle was affixed to the syringe, which was then mounted onto an ISO 7886-1 Syringe Compression Fixture attached to a manual test stand model TSB100 (Mark-10). A Series 5 advanced digital force gauge, equipped with a flat head, was also attached to the test stand to measure the compression force exerted on the syringe. The peak force required to expel the gel from the needle tip was recorded at least three times for each time point for accuracy.

Degradation Study: 100 µL of the mixed pre-gel HAMC solution with and without PLGA nanoparticles was dispensed into pre-weighed 2 mL Eppendorf tubes and then incubated at 37 °C to ensure complete gelation. The following day, the tubes containing the gels were weighed, and 900 µL of PBS with 400 U mL^{-1} of hyaluronidase was added to each tube. At designated time points, the supernatant was carefully removed to avoid disturbing the gel, and the tubes were re-weighed. The degradation of the hydrogels was determined by calculating the ratio of the hydrogel mass at each time point to its initial mass.

Animal Approval: All animal work was approved by the Animal Care Committee at the University of Toronto and was performed in accordance with the Guide to the Care and Use of Experimental Animals (Canadian Council on Animal Care).

Stroke Surgeries and Injection of Drug Delivery Vehicle: A total of 118 C57BL/6 mice (male, age 9–11 weeks) were used in this study (Charles River, Quebec City, Canada). Mice were anesthetised with isoflurane, shaved, and placed into a Kopf stereotaxic instrument. The scalp was cleaned with ethanol and chlorhexidine, and a midline incision was made, exposing the skull. A 2.3 mm diameter burr hole centered at 2.25 mm mediolateral (ML) and 0.6 mm anteroposterior (AP) relative to bregma was made in the skull. 1 µL of the vasoconstrictor endothelin-1 (800 pM, Abcam, ab120471) was injected at 2.25 mm ML, 0.6 mm AP, and 1.0 mm dorsoventral relative to bregma at 0.1 µL min^{-1}. After injection, the needle was left in place for 2.5 min before removal to limit backflow. Following this, for PACAP-treated mice, a 5.9 mm diameter polycarbonate disk with a 2 mm diameter opening was fixed over the burr hole using bone glue (Henkel Corporation, Loctite 454), and 3 µL of PACAP loaded drug delivery composite was injected by hand onto the surface of the brain using a Hamilton syringe (accurate to 0.1 µL) and equipped with a 26G needle. A second polycarbonate disk with no opening was secured on top of the first with bone glue. For vehicle-only mice, the surgery was performed as described, except a blank hydrogel-nanoparticle composite was injected onto the surface of the brain instead. For injury only mice, a 2.3 mm diameter circle of medical-grade silicone sheeting (BioPlexus, CUST-20001-005) was placed into the burr hole onto the surface of the brain, a small amount of Surgifoam gelatin sponge (Ethicon, 1972) was added on top, and the hole sealed with Ortho-Jet™ BCA dental cement (Lang Dental, 1334CLR). For sham mice, the scalp was shaved, cleaned with ethanol and chlorhexidine, and a midline incision was made, exposing the skull. All mice had their skin sutured and recovered on a heating pad prior to moving to cages.

Behavioral Testing and Training: The horizontal ladder assay and grip strength assessment were used to measure forelimb function. In the horizontal ladder assay, mice were trained daily for 3 d prior to stroke injury. A horizontal ladder was constructed 5 cm wide with clear, 1 cm thick acrylic walls. The walls had 60 rung holes spaced 1 cm apart, and 36 rungs were irregularly placed across the ladder. Ladder rung placement was the same for all mice. Mice were filmed walking across the ladder 3 times in the same direction (roughly 20–30 steps per run for a total of 60+ steps) (Video S1, Supporting Information). Baseline performance was calculated from the 3 runs of the last day of training prior to the stroke surgery. Slips of the forepaws, and total steps were counted by a blinded scorer. A slip was counted if the paw dropped below the ladder rungs. For grip strength, mice were held by the base of the tail and positioned to grab a T-bar connected to a BIO-GS3 grip strength test (BIOSEB, Pinellas Park, USA) with their front paws. When a firm grip was established, the mouse was pulled with a force parallel to the T-bar from the base of the tail. The strength at which the mouse let go of the T-bar was recorded as maximum grip strength with 4 replicates and normalized to baseline grip strength that was calculated from 4 replicates the day prior to stroke surgery. On 2, 4, 9, 18, and 28 d post stroke, mice were assessed with both the horizontal ladder and grip strength assays. Forepaw slips from the horizontal ladder assay was normalized to the baseline performance for each mouse and calculated as in Equation (1):

$$\%\text{slip} = \frac{\text{number of forepaw slips}}{\text{total steps taken}} - \frac{\text{baseline number of forepaw slips}}{\text{baseline total steps taken}} \quad (1)$$

Grip strength was normalized to each mouse's baseline grip strength and calculated as in Equation (2):

$$\text{grip strength} = \frac{\text{average grip strength}}{\text{baseline average grip strength}} \quad (2)$$

Mice were excluded from analysis if they did not exhibit a deficit at 2 days post-injury (dpi) in forepaw slips greater than 1 standard deviation of their own baseline. In total, five mice were excluded, one from the vehicle-treated group and two each from the injury group and PACAP group.

Brain Tissue Processing: Mice used for behavioral assessment were sacrificed at 28 d post-injury. Separate groups of mice were sacrificed at 4, 7, 10, 14 days post-injury. Mice were transcardially perfused with PBS, followed by cold (4 °C) 4% paraformaldehyde. Tissue was then cryoprotected until the tissue sank in 15% sucrose, followed by 30% sucrose at 4 °C. Cryoprotected brains were snap frozen in dry ice cold isopentane, and 25 µm thick coronal sections were taken from AP+3.0 to AP-1.5 relative to bregma.

Immunohistochemistry: For immunohistochemistry, coronal sections were allowed to equilibrate to RT, then permeabilized with 1% Tween20 in PBS for 15 min at RT. Sections were washed 3-times with PBS, then blocked with 10% donkey serum (Sigma–Aldrich, D9663), 0.1% Tween20 in PBS (block solution) for 1 h. Block solution was then removed, and sections were stained with primary antibodies (combination 1: rabbit anti-GFAP [1:500, Dako, Z033401-2], chicken anti-NeuN [1:500, Sigma–Aldrich, ABN91], goat anti-Iba1 [1:250, Novus Biologicals, NB100-1028SS], combination 2: rabbit anti-Iba1 [1:1000, Wako Chemicals, 019-19741], rat anti-CD86 [1:200, Abcam, ab119857], chicken anti-Arg1 [1:250, Sigma–Aldrich, ABS535], combination 3: chicken anti-GFAP [1:500, Abcam, ab4674], goat anti-LCN2 [1:200, Novus Biologicals, AF1857], rabbit anti-S100β [ready to use, Dako, IR504]), in block solution overnight at 4 °C. The next day, sections were washed 3-times with PBS, and stained with secondary antibodies (combination 1: donkey anti-rabbit 647 [ThermoFisher, A31573], donkey anti-goat 555 [ThermoFisher, A32816], donkey anti-chicken 488 [Sigma Aldrich, SAB4600031], combination 2: donkey anti-chicken 647 [Jackson ImmunoResearch, 703-605-155], goat anti-rabbit 546 [ThermoFisher, A11035], donkey anti-rat 488 [ThermoFisher, A21208], combination 3: donkey anti-chicken 488 [Sigma Aldrich, SAB4600031], donkey anti-goat 555 [ThermoFisher, A32816], donkey anti-rabbit 647 [ThermoFisher, A31573]), and Hoechst (ThermoFisher, 62249), all at 1:500 in block solution for 1 h at RT. Sections were washed 3-times with PBS, then mounted with ProLong™ Gold Antifade Mountant (ThermoFisher P36930) for imaging.

TUNEL and NeuN Staining: Terminal deoxynucleotidyl transferase dUTP nick end labeling (TUNEL) was used to assess apoptosis. For TUNEL staining, coronal sections were allowed to equilibrate to RT, then permeabilized with 1% TritonX in PBS for 15 min at RT. Sections were washed 3 times with PBS, the stained using the In Situ Cell Death Detection Kit, TMR red (Roche, 12156792910), following manufacturer instructions. Then, sections were washed 3 times with PBS and blocked with block solution for 1 h. Block solution was then removed, and sections were stained with chicken anti-NeuN [1:500, Sigma Aldrich, ABN91] in block solution overnight at 4 °C. The next day, sections were washed 3 times with PBS, and stained with donkey anti-chicken 488 [1:500, Sigma Aldrich, SAB4600031] in block solution for 1 h at RT. Sections were washed 3 times with PBS, then mounted with ProLong™ Gold Antifade Mountant (ThermoFisher P36930) for imaging.

Brain Tissue Imaging: Images were taken with a 20X objective on an Axio Scan.Z1 Slidescanner (Zeiss, Oberkochen, Germany).

Infarct Volume Measurement: Coronal sections spaced 250 µm apart between AP+1.6 and AP-0.4 relative to bregma were assessed for each mouse (Image of brain harvested at 4 dpi shown in Figure S1, Supporting Information). Infarct border was defined by the transition from dense NeuN staining to sparse/no NeuN staining ($NeuN^{dense}/NeuN^{sparse}$ border), and infarct area was calculated for each section (infarct ROI) (Representative image in Figure S2, Supporting Information). The pixel area of this region of interest (ROI) was converted to μm^2, and the volume between 2 sections (250 µm apart) was calculated by converting the area of each section to a circle and forming a truncated cone with a 250 µm height, and summing all volumes over AP+1.6 to AP-0.4 for each mouse. The infarct areas were drawn by a blinded experimenter.

TUNEL and NeuN Staining Quantification: Coronal sections spaced 250 µm apart between AP+1.6 and AP-0.4 relative to bregma were assessed for each mouse. Using the infarct ROI as described previously, a custom Python script was used to define two perilesional areas 250 and 500 µm away from the infarct border (0–250 µm perilesion ROI, and 250–500 µm perilesion ROI, respectively). The ndimage.morphology.binary_dilation package was used to dilate the lesion area 250 µm twice to define the perilesional areas: the inner ROI is comprised of 0–250 um, and the outer ROI comprised the 250–500 um (Representative image in Figure S2, Supporting Information). Using the Hoechst staining channel, regions of the image only containing tissue was defined and used as a mask on the lesional and perilesional ROIs. A Gaussian blur and top-hat transform, followed by the Otsu thresholding algorithm (all from skimage), was used to threshold the images and convert them to a binary image. Cell counting for $TUNEL^+$, NeuN+, and $TUNEL^+NeuN^+$ co-labelled cells was performed using the skimage.measure.label package on a binary image, counting cells greater than 16 or 50 μm^2 for $TUNEL/TUNEL^+NeuN^+$ and NeuN staining, respectively, in all of the ROIs (sum of cells in the infarct ROI, 0–250 µm perilesion ROI, and 250–500 µm perilesion ROI).

Astrocyte and Microglia Quantification: Astrocyte and microglia activation were calculated based on $GFAP^+$ and $Iba1^+$ staining, respectively. Coronal sections spaced 250 µm apart between AP+1.6 and AP-0.4 relative to bregma were assessed for each mouse. Similar processing defined above was performed for GFAP and Iba1 staining for the infarct ROI, 0–250 µm perilesion ROI, and 250–500 µm perilesion ROI. After the images were converted to binary as stated previously, the sum of all positive pixels in each specific ROI was calculated and divided by the area of the ROI (the Hoechst mask was used to subtract area that did not include tissue) to determine the %positive pixels, and this value divided by the sum of all positive pixels in an ROI in the contralateral hemisphere ÷ contralateral ROI area to determine the staining intensity (Equation 3).

$$\begin{aligned}&\text{staining intensity normalized to contralateral}\\ &= \frac{\text{number of positive pixels in ROI}}{\text{ROI area in Hoechst mask}}\\ &\times \frac{\text{contralateral ROI area in Hoechst mask}}{\text{number of positive pixels in contralateral ROI}}\end{aligned} \quad (3)$$

Microglia Polarization Quantification: Microglia activation was characterized by CD86 and Arg1 staining. Coronal sections spaced 250 µm apart between AP+1.6 and AP-0.4 relative to bregma were assessed for each mouse. An ROI containing all activated ameboid microglia stained with Iba1 was drawn by a blinded experimenter in a similar manner to the infarct ROI. Images were processed as previously described for co-labelled $CD86^+Iba1^+$ staining, and co-labelled $Arg1^+Iba1^+$ staining for the activated ameboid microglia ROI.

Astrocyte Activation Quantification: Astrocyte activation was characterized by LCN2 and S100β staining. Coronal sections spaced 250 µm apart between AP+1.6 and AP-0.4 relative to Bregma were assessed for each mouse. An ROI containing activated astrocytes stained with GFAP was drawn by a blinded experimenter in a similar manner to the microglia polarization ROI. Images were then processed in ZEN Blue (ZEISS, version 3.10) using the colocalization function to assess the relative area (%) of $GFAP^+LCN2^+$ and $GFAP^+$ $S100\beta^+$ within the $GFAP^+$ ROI. Thresholding was performed on each image individually by referencing the background tissue staining intensity of the contralateral brain.

Statistical Analysis: All statistical analyses were performed using GraphPad Prism software version 7. Behavioral testing was analyzed using two-way repeated measures analysis of variance (ANOVA), followed by Tukey's post hoc test for multiple comparisons. Infarct volume, TUNEL staining, $CD86^+Iba1^+$ staining, and $Arg1^+Iba1^+$ staining were analyzed using one-way (ANOVA), followed by Tukey's post hoc test for multiple comparisons for each timepoint. Iba1 and GFAP staining were analyzed

using two-way ANOVA, followed by Tukey's post hoc test for multiple comparisons for each separate ROI. Astrocyte activation staining was analyzed using two-way ANOVA, followed by Tukey's post hoc test for multiple comparisons. Significance was defined as $p<0.05$.

Supporting Information

Supporting Information is available from the Wiley Online Library or from the author.

Acknowledgements

The authors are grateful for funding from the Canadian Institutes for Health Research (CIHR) and the Natural Science and Engineering Research Council (NSERC) for funding through the Collaborative Health Research Program (CHRP to CMM and MSS). The authors are grateful for additional support: NSERC PGSD to EH, NSERC Vanier CGS to DXL, Discovery and Herzberg Gold Medal to MSS. The authors thank: Dr. Rainerio De Guzman and Dr. Jean Kontogiannis for assistance in surgery preparations, Dr. Lindsey Fiddes for assistance with IHC imaging, and members of the Shoichet lab for their thoughtful review of this manuscript.

Conflict of Interest

The authors declare no conflict of interest.

Author Contributions

E.H. and M.S.S. conceived the project and designed the experiments. E.H., D.X.L., and M.S.S. interpreted the results and wrote the manuscript. E.H. performed most of the experiments. D.X.L. performed astrocyte activation experiments and material characterization. H.C. assisted in animal surgeries and tissue collection. D.X.L. and D.A. assisted in the tissue collection and processing. R.S. and C.M.M. provided advice on stroke studies, tissue analysis, and behavioral testing. D.C. provided advice on PACAP.

Data Availability Statement

The data that support the findings of this study are available from the corresponding author upon reasonable request.

Keywords

astrocytes, electrostatic controlled release, hydrogel, inflammation, microglia, nanoparticle, PACAP, pituitary adenylate cyclase activating polypeptide, stroke

Received: February 11, 2025
Revised: June 26, 2025
Published online:

[1] C. W. Tsao, A. W. Aday, Z. I. Almarzooq, C. A. M. Anderson, P. Arora, C. L. Avery, C. M. Baker-Smith, A. Z. Beaton, A. K. Boehme, A. E. Buxton, Y. Commodore-Mensah, M. S. V. Elkind, K. R. Evenson, C. Eze-Nliam, S. Fugar, G. Generoso, D. G. Heard, S. Hiremath, J. E. Ho, R. Kalani, D. S. Kazi, D. Ko, D. A. Levine, J. Liu, J. Ma, J. W. Magnani, E. D. Michos, M. E. Mussolino, S. D. Navaneethan, N. I. Parikh, *Circulation* **2023**, *147*, E93.
[2] U. Fischer, J. Kaesmacher, V. M. Pereira, R. Chapot, A. H. Siddiqui, M. T. Froehler, C. Cognard, A. J. Furlan, J. L. Saver, J. Gralla, *Stroke* **2017**, *48*, 2912.
[3] A. P. Jadhav, S. M. Desai, T. G. Jovin, *Neurology* **2021**, *97*, S126.
[4] X. Y. Xiong, L. Liu, Q. W. Yang, *Prog. Neurobiol.* **2016**, *142*, 23.
[5] Y. Ma, J. Wang, Y. Wang, G. Y. Yang, *Prog. Neurobiol.* **2017**, *157*, 247.
[6] M. Kawabori, M. Yenari, *Curr. Med. Chem.* **2015**, *22*, 1258.
[7] L. Huang, Z. B. Wu, Q. ZhuGe, W. Zheng, B. Shao, B. Wang, F. Sun, K. Jin, *Int. J. Med. Sci.* **2014**, *11*, 344.
[8] M. V. A Sofroniew, *Cold Spring Harb. Perspect. Biol.* **2015**, *7*, a020420.
[9] R. Guruswamy, A. Elali, *Int. J. Mol. Sci.* **2017**, *18*, 496.
[10] G. T. Manley, Z. Zador, S. Stiver, V. Wang *Handbook of Experimental Pharmacology*, Springer, Berlin, **2009**, 159–170.
[11] G. M. Smith, C. Strunz, *Glia* **2005**, *52*, 209.
[12] G. J. Del Zoppo, R. Milner, T. Mabuchi, S. Hung, X. Wang, G. I. Berg, J. A. Koziol, *Stroke* **2007**, *38*, 646.
[13] A. Otxoa-de-Amezaga, F. Miró-Mur, J. Pedragosa, M. Gallizioli, C. Justicia, N. Gaja-Capdevila, F. Ruíz-Jaen, A. Salas-Perdomo, A. Bosch, M. Calvo, L. Márquez-Kisinousky, A. Denes, M. Gunzer, A. M. Planas, *Acta Neuropathol.* **2019**, *137*, 321.
[14] G. Szalay, B. Martinecz, N. Lénárt, Z. Környei, B. Orsolits, L. Judák, E. Császár, R. Fekete, B. L. West, G. Katona, B. Rózsa, Á. Dénes, *Nat. Commun.* **2016**, *7*, 11499.
[15] M. Lalancette-Hébert, G. Gowing, A. Simard, C. W. Yuan, J. Kriz, *J. Neurosci.* **2007**, *27*, 2596.
[16] M. V. Sofroniew, H. V. Vinters, *Acta Neuropathol.* **2010**, *119*, 7.
[17] A. J. Gleichman, S. T. Carmichael, *Neurosci. Lett.* **2014**, *565*, 47.
[18] Y. Tang, W. Le, *Mol. Neurobiol.* **2016**, *53*, 1181.
[19] D. Nowicka, K. Rogozinska, M. Aleksy, O. W. Witte, J. Skangiel-Kramska, *Acta Neurobiol. Exp. (Wars)*. **2008**, *68*, 155.
[20] A. R. Patel, R. Ritzel, L. D. McCullough, F. M Liu, I. S. A. D.-E. Sword, *Int. J. Physiol. Pathophysiol. Pharmacol.* **2013**, *5*, 73.
[21] C. Y. Xia, S. Zhang, Y. Gao, Z. Z. Wang, N. H. Chen, *Int. Immunopharmacol.* **2015**, *25*, 377.
[22] N. Letko Khait, E. Ho, M. S. Shoichet, N. Letko Khait, E. Ho, M. S. Shoichet, *Adv. Funct. Mater.* **2021**, *31*, 2010674.
[23] Y. Lu, M. Zhou, Y. Li, Y. Li, Y. Hua, Y. Fan, *Biochem. Pharmacol.* **2021**, *186*, 114464.
[24] C. Bourget, K. V. Adams, C. M. Morshead, *J. Neuroinflammation* **2022**, *19*, 1.
[25] A. Arimura, A. Somogyvàri-Vigh, A. Miyata, K. Mizuno, D. H. Coy, C. Kitada, *Endocrinology* **1991**, *129*, 2787.
[26] R. Stumm, A. Kolodziej, V. Prinz, M. Endres, D.-F. Wu, V. Höllt, *J. Neurochem.* **2007**, *103*, 1666.
[27] D. Tsuchikawa, T. Nakamachi, M. Tsuchida, Y. Wada, M. Hori, J. Farkas, A. Yoshikawa, N. Kagami, N. Imai, N. Shintani, H. Hashimoto, T. Atsumi, S. Shioda, *J. Mol. Neurosci.* **2012**, *48*, 508.
[28] M. Nishimoto, H. Miyakawa, K. Wada, A. Furuta, *Brain Res.* **2011**, *1383*, 43.
[29] A. Dejda, T. Seaborn, S. Bourgault, O. Touzani, A. Fournier, H. Vaudry, D. Vaudry, *Peptides* **2011**, *32*, 1207.
[30] M. Delgado, J. Leceta, D. Ganea, *J. Leukoc. Biol.* **2003**, *73*, 155.
[31] I. Tatsuno, H. Morio, T. Tanaka, D. Uchida, A. Hirai, Y. Tamura, Y. Saito, *Ann. N. Y. Acad. Sci.* **1996**, *805*, 482.
[32] H. Ohtaki, T. Nakamachi, K. Dohi, Y. Aizawa, A. Takaki, K. Hodoyama, S. Yofu, H. Hashimoto, N. Shintani, A. Baba, M. Kopf, Y. Iwakura, K. Matsuda, A. Arimura, S. Shioda, *Proc. Natl. Acad. Sci. USA* **2006**, *103*, 7488.
[33] P. Lazarovici, G. Cohen, H. Arien-Zakay, J. Chen, C. Zhang, M. Chopp, H. Jiang, *J. Mol. Neurosci.* **2012**, *48*, 526.
[34] D. Reglodi, A. Somogyvari-Vigh, S. Vigh, T. Kozicz, A. Arimura, *Stroke* **2000**, *31*, 1411.
[35] C. Brifault, M. Gras, D. Liot, V. May, D. Vaudry, O. Wurtz, *Stroke* **2015**, *46*, 520.

[36] D. Uchida, A. Arimura, A. Somogyvári-Vigh, S. Shioda, W. A. Banks, *Brain Res.* **1996**, *736*, 280.
[37] J. A. Waschek, *Br. J. Pharmacol.* **2013**, *169*, 512.
[38] S. Shioda, T. Nakamachi, *Peptides* **2015**, *72*, 202.
[39] K. Dohi, H. Mizushima, S. Nakajo, H. Ohtaki, S. Matsunaga, T. Aruga, S. Shioda, *Regul. Pept.* **2002**, *109*, 83.
[40] R. A. Stetler, Y. Gao, R. S. Zukin, P. S. Vosler, L. Zhang, F. Zhang, G. Cao, M. V. L. Bennett, J. Chen, *Proc. Natl. Acad. Sci. USA* **2010**, *107*, 3204.
[41] M. Hori, T. Nakamachi, R. Rakwal, J. Shibato, T. Ogawa, T. Aiuchi, T. Tsuruyama, K. Tamaki, S. Shioda, *J. Neuroinflammation* **2012**, *9*, 256.
[42] D. Reglodi, Z. Fábián, A. Tamás, A. Lubics, J. Szeberényi, T. Alexy, K. Tóth, Z. Márton, B. Borsiczky, E. Roth, L. Szalontay, I. Lengvári, *Regul. Pept.* **2004**, *123*, 51.
[43] O. Farkas, A. Tamás, A. Zsombok, D. Reglodi, J. Pál, A. Büki, I. Lengvári, J. T. Povlishock, T. Dóczi, *Regul. Pept.* **2004**, *123*, 69.
[44] W. M. Pardridge, *Fluids Barriers CNS* **2011**, *8*, 7.
[45] M. D. Baumann, C. E. Kang, J. C. Stanwick, Y. Wang, H. Kim, Y. Lapitsky, M. S. Shoichet, *J. Controlled Release* **2009**, *138*, 205.
[46] E. Ho, Y. Deng, D. Akbar, K. Da, M. Létourneau, C. M. Morshead, D. Chatenet, M. S. Shoichet, *Cite This ACS Appl. Mater. Interfaces* **2023**, *15*, 91.
[47] M. D. Baumann, C. E. Kang, C. H. Tator, M. S. Shoichet, *Biomaterials* **2010**, *31*, 7631.
[48] D. Gupta, C. H. Tator, M. S. Shoichet, *Biomaterials* **2006**, *27*, 2370.
[49] M. M. Pakulska, I. Elliott Donaghue, J. M. Obermeyer, A. Tuladhar, C. K. McLaughlin, T. N. Shendruk, M. S. Shoichet, *Nanoparticles. Sci. Adv.* **2016**, *2*, 1.
[50] M. Ye, S. Kim, K. Park, *J. Controlled Release* **2010**, *146*, 241.
[51] H. K. Makadia, S. J. Siegel, *Polymers (Basel)* **2011**, *3*, 1377.
[52] K. E. Fifield, J. L. Vanderluit, *Eur. J. Neurosci.* **2020**, *52*, 3196.
[53] R. B. Roome, R. F. Bartlett, M. Jeffers, J. Xiong, D. Corbett, J. L. Vanderluit, *J. Neurosci. Methods* **2014**, *233*, 34.
[54] T. E. Robinson, E. A. B. Hughes, A. Bose, E. A. Cornish, J. Y. Teo, N. M. Eisenstein, L. M. Grover, S. C. Cox, *Adv. Healthcare Mater.* **2020**, *9*, 1901521.
[55] K. A. Tennant, T. A. Jones, *J. Neurosci. Methods* **2009**, *181*, 18.
[56] S. L. Payne, A. Tuladhar, J. M. Obermeyer, B. V Varga, C. J. Teal, C. M. Morshead, A. Nagy, M. S. Shoichet, *Biomaterials* **2019**, *192*, 309.
[57] N. Saunders, M. Habgood, K. Dziegielewska, *Clin. Exp. Pharmacol. Physiol.* **1999**, *26*, 11.
[58] S. Wohlfart, S. Gelperina, J. Kreuter, *J. Controlled Release* **2012**, *161*, 264.
[59] Y. Wang, M. J. Cooke, N. Sachewsky, C. M. Morshead, M. S. Shoichet, *J. Controlled Release* **2013**, *172*, 1.
[60] J. M. Obermeyer, A. Tuladhar, S. L. Payne, E. Ho, C. M. Morshead, M. S. Shoichet, *Tissue Eng. Part A.*, *25*, 1175, https://doi.org/10.1089/ten.TEA.2018.0215.
[61] J. W. Austin, C. Gilchrist, M. G. Fehlings, *J. Neurochem.* **2012**, *122*, 344.
[62] C. Cooper, K. K. Brown, C. D. Meletis, N. I. Zabriskie, H. Acid, *Altern. Complement. Ther.* **2008**, *14*, 78.
[63] J. A. Burdick, G. D. Prestwich, *Adv. Mater.* **2011**, *23*, H41.
[64] A. Tuladhar, J. M. Obermeyer, S. L. Payne, R. C. W. Siu, S. Zand, C. M. Morshead, M. S. Shoichet, *Biomaterials* **2020**, *235*, 119794.
[65] D. Kim, J. W. Lee, Y. T. Kim, J. Choe, G. Kim, C. M. Ha, J. G. Kim, K. H. Song, S. Yang, *Adv. Healthc. Mater.* **2025**, *14*, 2403119.
[66] M. Delgado, G. M. Jonakait, D. Ganea, *Glia* **2002**, *39*, 148.
[67] D. A. Wainwright, J. Xin, V. M. Sanders, K. J. Jones, *J. Neurodegener. Regen.* **2008**, *1*, 31.
[68] A. Cherait, J. Maucotel, B. Lefranc, J. Leprince, D. Vaudry, *Front. Endocrinol. (Lausanne)*. **2021**, *11*, 585082.
[69] O. Masmoudi-Kouki, P. Gandolfo, H. Castel, J. Leprince, A. Fournier, A. Dejda, H. Vaudry, M. C. Tonon, *Peptides* **2007**, *28*, 1753.
[70] S. Douiri, S. Bahdoudi, Y. Hamdi, R. Cubì, M. Basille, A. Fournier, H. Vaudry, M. C. Tonon, M. Amri, D. Vaudry, O. Masmoudi-Kouki, *J. Neurochem.* **2016**, *137*, 913.
[71] D. Vaudry, T. F. Pamantung, M. Basille, C. Rousselle, A. Fournier, H. Vaudry, J. C. Beauvillain, B. J. Gonzalez, *Eur. J. Neurosci.* **2002**, *15*, 1451.
[72] D. Vaudry, A. Falluel-Morel, M. Basille, T. F. Pamantung, M. Fontaine, A. Fournier, H. Vaudry, B. J. Gonzalez, *J. Neurosci. Res.* **2003**, *72*, 303.
[73] J. D. Cherry, J. A. Olschowka, M. K. O'Banion, *J. Neuroinflammat.* **2014**, *11*, 98.
[74] A. Q. Chen, Z. Fang, X. L. Chen, S. Yang, Y. F. Zhou, L. Mao, Y. P. Xia, H. J. Jin, Y. N. Li, M. F. You, X. X. Wang, H. Lei, Q. W. He, B. Hu, *Cell Death Dis.* **2019**, *10*, 487.
[75] S. Murphy, M. L. Simmons, L. Agullo, A. Garcia, D. L. Feinstein, E. Galea, D. J. Reis, D. Minc-Golomb, J. P. Schwartz, *Trends Neurosci.* **1993**, *16*, 323.
[76] C. A. Moraes, G. Santos, T. C. L. S. Spohr, D' J. C. Avila, F. R. S. Lima, C. F. Benjamim, F. A. Bozza, F. C. A. Gomes, *Mol. Neurobiol.* **2015**, *52*, 653.
[77] D. Battista, C. C. Ferrari, F. H. Gage, F. J. Pitossi, *Eur. J. Neurosci.* **2006**, *23*, 83.
[78] S. Y. Park, H. Lee, J. Hur, S. Y. Kim, H. Kim, J. H. Park, S. Cha, S. S. Kang, G. J. Cho, W. S. Choi, K. Suk, *Mol. Brain Res.* **2002**, *107*, 9.
[79] P. E. Batchelor, G. T. Liberatore, J. Y. F. Wong, M. J. Porritt, F. Frerichs, G. A. Donnan, D. W. Howells, *J. Neurosci.* **1999**, *19*, 1708.
[80] X. Hu, R. K. Leak, Y. Shi, J. Suenaga, Y. Gao, P. Zheng, J. Chen, *Nat. Rev. Neurol.* **2015**, *11*, 56.
[81] H. Wake, A. J. Moorhouse, S. Jinno, S. Kohsaka, J. Nabekura, *J. Neurosci.* **2009**, *29*, 3974.
[82] R. C. Paolicelli, G. Bolasco, F. Pagani, L. Maggi, M. Scianni, P. Panzanelli, M. Giustetto, T. A. Ferreira, E. Guiducci, L. Dumas, D. Ragozzino, C. T. Gross, *Science* **2011**, *333*, 1456.
[83] W. K. Kim, Y. Kan, D. Ganea, R. P. Hart, I. Gozes, G. M. Jonakait, *J. Neurosci.* **2000**, *20*, 3622.
[84] S. Yang, J. Yang, Z. Yang, P. Chen, A. Fraser, W. Zhang, H. Pang, X. Gao, B. Wilson, J. S. Hong, M. L. Block, *J. Pharmacol. Exp. Ther.* **2006**, *319*, 595.
[85] K. Suk, J. H. Park, W. H. Lee, *Brain Res.* **2004**, *1026*, 151.
[86] Y. Wada, T. Nakamachi, K. Endo, T. Seki, H. Ohtaki, D. Tsuchikawa, M. Hori, M. Tsuchida, A. Yoshikawa, A. Matkovits, N. Kagami, N. Imai, S. Fujisaka, I. Usui, K. Tobe, R. Koide, H. Takahashi, S. Shioda, *J. Mol. Neurosci.* **2013**, *51*, 493.
[87] M. Kawabori, M. A. Yenari, *Curr. Med. Chem.* **2015**, *22*, 1258.
[88] G. Barreto, R. E. White, Y. Ouyang, L. Xu, R. G. Giffard, *Cent. Nerv. Syst. Agents Med. Chem.* **2012**, *11*, 164.
[89] Q. Tan, C. Zhang, X. Rao, W. Wan, W. Lin, S. Huang, J. Ying, Y. Lin, F. Hua, *Front. Immunol.* **2024**, *15*, 1358719.
[90] S. Lee, M. K. Jha, K. Suk, *Crit. Rev. Immunol.* **2015**, *35*, 77.
[91] R. Donato, G. Sorci, R. Bianchi, F. Riuzzi, C. Tubaro, C. Arcuri, *Cardiovasc. Psychiatry Neurol.* **2010**, *2010*, 656481.
[92] F. Michetti, N. D'Ambrosi, A. Toesca, M. A. Puglisi, A. Serrano, E. Marchese, V. Corvino, M. C. Geloso, *J. Neurochem.* **2019**, *148*, 168.
[93] H. Kato, A. Ito, J. Kawanokuchi, S. Jin, T. Mizuno, K. Ojika, R. Ueda, A. Suzumura, *Mult. Scler.* **2004**, *10*, 651.
[94] D. Reglodi, P. Kiss, A. Lubics, A. Tamas, *Curr. Pharm. Des.* **2011**, *17*, 962.
[95] D. Reglodi, A. Lubics, A. Tamás, L. Szalontay, I. Lengvári, *Behav. Brain Res.* **2004**, *151*, 303.
[96] S. Hickman, S. Izzy, P. Sen, L. Morsett, J. El Khoury, *Nat. Neurosci.* **2018**, *21*, 1359.
[97] Y. Xu, M. Z. Jin, Z. Y. Yang, W. L. Jin, *Neural Regener. Res.* **2021**, *16*, 270.
[98] H. J. Yoo, M. S. Kwon, *Front. Aging Neurosci.* **2022**, *13*, 928.